Available online at www.sciencedirect.com

ScienceDirect

Materials Today: Proceedings 5 (2018) 7410–7419

materialstoday: PROCEEDINGS

www.materialstoday.com/proceedings

IMME17

Influence of Coupled Material Properties of $BaTiO_3$ and $CoFe_2O_4$ on the Static Behavior of Thermo-Mechanically Loaded Magneto-Electro-Elastic Beam

Vinyas. M[a], S.C. Kattimani[a]*

[a]*Department of Mechanical Engineering, National Institute of Technology Karnataka, Surathkal-575025, India*

Abstract

The present article deals with analyzing the influence of volume fraction (V_f) of Barium Titanate ($BaTiO_3$) and Cobalt-Ferric oxide ($CoFe_2O_4$) and its corresponding coupled material properties on the static response of multiphase magneto-electro-elastic (MEE) cantilever beam. Using finite element (FE) methods, the variations of direct and derived quantities across the beam thickness are evaluated. The different volume fractions ranging from $V_f = 0.0$ to $V_f = 1.0$ are considered for analysis. The equilibrium equations are presented with the help of the total potential energy principle and coupled constitutive equations of MEE materials. The numerical results suggest that the displacement components vary accordingly with the volume fraction. In addition, it is found that the maximum electric potential is observed for $V_f = 0.2$ due to pyro-effects, whereas maximum magnetic potential is obtained for $V_f = 0.0$. The numerical study is extended to analyse the layered MEE beam. The influence of stacking sequence and different mechanical load forms on the direct quantities of the beam is evaluated. It is believed that for the precise design of any smart structure, the credibility of the material properties plays a significant role. Hence, in this regard an attempt has been made to understand the behavior of multiphase MEE beams with respect to different volume fractions of Barium titanate ($BaTiO_3$) and Cobalt-Ferric oxide ($CoFe_2O_4$).

Selection and/or Peer-review under responsibility of International Conference on Emerging Trends in Materials and Manufacturing Engineering (IMME17).

Keywords: magneto-electro-elastic; volume fraction; direct quantities; thermo-mechanical loads

* Corresponding author. Tel.: Tel.: +91-824-2473661;
E-mail address: sck@nitk.ac.in

Selection and/or Peer-review under responsibility of International Conference on Emerging Trends in Materials and Manufacturing Engineering (IMME17).

Nomenclature

V_f	Volume fraction of Barium Titanate ($BaTiO_3$) and Cobalt Ferric oxide ($CoFe_2O_4$)
L	Length of the magneto-electro-elastic beam
b	Width of the magneto-electro-elastic beam
h	Thickness of the magneto-electro-elastic beam
ψ	Magnetic potential
ϕ	Electric potential

1. Introduction

A remarkable influence of smart materials in many applications is recognized from the past few decades. Among them, a unique combination of piezoelectric and piezomagnetic materials commonly termed as magneto-electro-elastic (MEE) materials has gained much of the attention of researchers. The main constituents of the MEE materials are Barium Titanate ($BaTiO_3$) and Cobalt Ferric oxide ($CoFe_2O_4$). The maximum utilization of these materials in various fields has created a curiosity and necessity to study and analyse the coupled behavior of structures constructed with such smart materials. In addition, it displays noticeable capabilities such as self-sensing, self-actuating, reliability and all other performances demanded in modern sophisticated structural application. The magneto-electric coupling is considered as a cross product of the magneto-elastic and electro-elastic coupling properties. This makes MEE materials exceptional to other smart materials and potentially applicable in the field of sensors, actuators and transducers. As a result the research community is showing an increased interest in understanding the MEE materials from the technological, chemical and mechanical points of view. In order to evaluate the MEE properties, micromechanical approach, asymptotic methods and homogenization method has been developed [1] – [3].

Over the past few decades, many of the researchers have devoted their study to develop mathematical models for analyzing the mechanical responses of MEE structures (plates, beams and shells). The commonly employed procedures like exact solution method, analytical solution method, finite element method, meshless method, state space approach etc. have exhibited its credibility in the free vibration analysis of MEE structures [4-12]. Further, Kattimani and Ray presented a FE formulation for the active control of geometrically non-linear vibrations for MEE plates [13] and doubly curved shells [14]. Also, they extended their investigation for the functionally graded plates [15]. Appealing to 3D formulation, the dynamic response study of MEE structures are carried out by Wu *et al.* [16] and Biju *et al.* [17]. Few articles gave insight on the problem of transient response of MEE structures [18]-[21]. Meanwhile, the static analysis of MEE structures has been carried out by few of the pioneers which established a platform for a broad research. Among them, Phoenix *et al.* [22] used Reissner mixed variational theorem to analyse the static and dynamic behavior of the coupled MEE plates. Davi *et al.* [23] used boundary element approach and analysed the effect of magnetic configuration on the behavior of MEE bimorph beams. Lage *et al.* [24] studied the static behavior with the aid of semi-analytical FE formulation. More often, the MEE structures are required to perform in the thermal environment. In the presence of thermal environment, a drastic transition in the behavior of MEE structures can be observed in terms of displacements, potentials and stresses. Hence the study of these materials in thermal environment is essential. Using two energy functionals, Sunar *et al.* [25] derived the thermodynamic potential and its corresponding finite element formulation for fully coupled thermopiezomagnetic continuum. Badri and Kayiem [26] adopted the first order shear deformation theory (FSDT) to analyse the static and dynamic analysis of magneto-thermo-electro-elastic (MTEE) plates. Tauchert [27] developed an exact solution to study the effect of steady state temperature distribution on piezo thermoelastic problem. Ebrahimi and Barati [28] have evaluated the effect of the various temperature distributions on the frequency characteristics of magneto-electro-thermo-elastic functionally graded (METE-FG) nanobeams. They also studied the thermo-electro-mechanical buckling behavior of functionally graded piezoelectric materials [29].These materials exhibit an additional coupling between thermo-magnetic and thermo-electric material properties which are generally known as pyromagnetic and pyroelectric effects, respectively. Kumaravel *et al.* [30] studied the static behavior of MEE strips

in the presence of both uniform and non-uniform temperature distributions. They neglected the influence of pyroeffects in their analysis. Further, Kondaiah *et al.* [31] analysed the pyroelectric and pyromagnetic effects on MEE cylindrical shells. They extended their investigation to MEE beams [32] and plates [33]. Recently, Vinyas and Kattimani [34] investigated the static behavior of stepped functionally graded MEE beam subjected to different thermal loads.

From the exhaustive literature survey, it is noticed that limited works have been published on the static behavior of MEE beam subjected to the combined effect of thermal and mechanical loads. Hence in this article, an attempt has been made to investigate the influence of volume fraction of Barium Titanate ($BaTiO_3$) and Cobalt Ferric oxide ($CoFe_2O_4$) on the static parameters varying across the thickness of a multiphase MEE beam. Also, effect of different mechanical load profiles on the displacement and potentials of the layered MEE beam is evaluated using FE procedures.

2. Problem description

Beam geometry

The schematic representation of a multiphase MEE cantilever beam is depicted in Fig. 1. The beam length *L,* width *b* and thickness *h* of the beam is measured with respect to the *x, y* and *z* directions of the Cartesian co-ordinate.

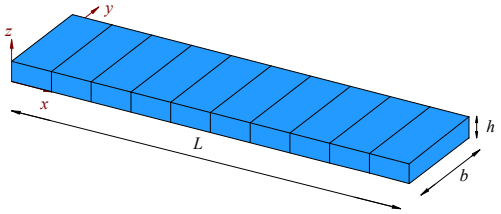

Fig. 1: Beam geometry

Constitutive equations

The coupled constitutive equations which establish a linear relationship between elastic, thermal, magnetic and electric properties of a MEE material can be represented as follows:

$$\sigma_i = C_{ij}(\varepsilon_j - \alpha_i \Delta T) - e_{ik}E_k - q_{ik}H_k \quad (1.a)$$

$$D_l = e_{lj}\,\varepsilon_j + \eta_{lk}E_k + m_{lk}H_k + p_k\Delta T \quad (1.b)$$

$$B_l = q_{lj}\varepsilon_j + m_{lk}E_k + \mu_{lk}H_k + \tau_k\Delta T \quad (1.c)$$

where i , j =1, 2…6 and l, k =1, 2, 3. In Eq. (1) σ_i, D_l and B_l represents the stress, electric displacement components and magnetic induction component, respectively. C_{ij}, η_{lk} and $\mu_{lk}$are the elastic constants, dielectric constants and magnetic permeability constant, respectively. ε_j, E_k, H_k and ΔT are the linear strain tensor, electric field, magnetic field and temperature rise, respectively. Further $e_{lj}, q_{lj}, m_{lk}, \alpha_i, p_k$ and τ_k are the piezoelectric, magnetostrictive, electromagnetic, thermal expansion co-efficient, pyroelectric constant and pyromagnetic constant, respectively. For a transversely isotropic MEE solid, the various material constants appearing in the constitutive equations (Eqs. 1(a) – (c)) can be represented in the matrix form as follows:

$$[C] = \begin{bmatrix} C_{11} & C_{12} & C_{13} & 0 & 0 & 0 \\ & C_{11} & C_{23} & 0 & 0 & 0 \\ & & C_{33} & 0 & 0 & 0 \\ & & & C_{44} & 0 & 0 \\ & Sym & & & C_{55} & 0 \\ & & & & & C_{66} \end{bmatrix}, [e]^T = \begin{bmatrix} 0 & 0 & 0 & 0 & e_{15} & 0 \\ 0 & 0 & 0 & e_{15} & 0 & 0 \\ e_{13} & e_{13} & e_{33} & 0 & 0 & 0 \end{bmatrix}$$

$$[q]^T = \begin{bmatrix} 0 & 0 & 0 & 0 & q_{15} & 0 \\ 0 & 0 & 0 & q_{15} & 0 & 0 \\ q_{13} & q_{13} & q_{33} & 0 & 0 & 0 \end{bmatrix}, [\mu] = \begin{bmatrix} \mu_{11} & 0 & 0 \\ 0 & \mu_{22} & 0 \\ 0 & 0 & \mu_{33} \end{bmatrix}, [m] = \begin{bmatrix} m_{11} & 0 & 0 \\ 0 & m_{22} & 0 \\ 0 & 0 & m_{33} \end{bmatrix}$$

$$[\eta] = \begin{bmatrix} \eta_{11} & 0 & 0 \\ 0 & \eta_{22} & 0 \\ 0 & 0 & \eta_{33} \end{bmatrix}, \{\alpha\} = \begin{Bmatrix} \alpha_1 \\ \alpha_2 \\ \alpha_3 \\ 0 \\ 0 \\ 0 \end{Bmatrix}, \{p\} = \begin{Bmatrix} p_1 \\ p_2 \\ p_3 \end{Bmatrix}, \{\tau\} = \begin{Bmatrix} \tau_1 \\ \tau_2 \\ \tau_3 \end{Bmatrix} \quad (2)$$

The strain field is related to the displacements as follows:

$$\varepsilon_{ij} = \frac{1}{2}\left(u_{i,j} + u_{j.i}\right) \quad (3)$$

The electric field vector (E) can be related to the electric potential (ϕ) as

$$E_1 = -\frac{\partial \phi}{\partial x};\ E_2 = -\frac{\partial \phi}{\partial y};\ E_3 = -\frac{\partial \phi}{\partial z} \quad (4)$$

Similarly, the relation between magnetic field vector (H) and magnetic potential (ψ) is expressed as

$$H_1 = -\frac{\partial \psi}{\partial x};\ H_2 = -\frac{\partial \psi}{\partial y};\ H_3 = -\frac{\partial \psi}{\partial z} \quad (5)$$

The total potential energy principle is evoked to derive the equilibrium equation as follows:

$$T_p = \frac{1}{2}\int_{\Omega}\{\varepsilon\}^T\{\sigma\}d\Omega - \frac{1}{2}\int_{\Omega}\{E\}^T\{D\}d\Omega - \frac{1}{2}\int_{\Omega}\{H\}^T\{B\}d\Omega - \int_A\{d_t\}^T\{f\}dA - \int_A \phi\ Q^{\phi}dA - \int_A \psi\ Q^{\psi}dA \quad (6)$$

where, T_p is the total potential energy of the system.

Finite element formulation

The MEE beam is discretized into 10 elements using eight noded 3D brick element as illustrated in Fig. 1. Each node is assumed to have five degrees of freedom *viz.* displacements in *x, y* and *z* direction, electric and magnetic potential. The nodal displacement, electric potential and magnetic potential can be expressed as follows:

$$u = [N_u]\{u_i\};\ \phi = [N_\phi]\{\phi_i\};\ \psi = [N_\psi]\{\psi_i\} \quad (7)$$

where, $\{u_i\} = \{u_x, u_v, u_w\}$ are the *x, y* and *z* direction displacement components , respectively. N_u, N_ϕ, N_ψ are the shape functions matrices. The corresponding strain vector, electric potential vector and magnetic potential vector can be obtained eventually in terms of Eq. (7) as follows:

$$\{\varepsilon\} = [B_u]\{u^{ele}\},\ \{H\} = [B_\psi]\{\psi^{ele}\},\ \{E\} = [B_\phi]\{\phi^{ele}\} \quad (8)$$

By substituting Eqs. (7) and (8) in Eq. (6), the coupled FE equilibrium equations of the MEE beam can be written as

$$\begin{aligned} &[K_{uu}]\{u^{ele}\} + [K^e_{u\phi}]\{\phi^{ele}\} + [K^e_{u\psi}]\{\psi^{ele}\} = \{F^e_m\} + \{F^e_{th}\} \\ &[K^e_{u\phi}]^T\{u^{ele}\} - [K^e_{\phi\phi}]\{\phi^{ele}\} - [K^e_{\phi\psi}]\{\psi^{ele}\} = \{F^e_\phi\} - \{F^e_{p.e}\} \\ &[K^e_{u\psi}]^T\{u^{ele}\} - [K^e_{\phi\psi}]^T\{\phi^{ele}\} - [K^e_{\psi\psi}]\{\psi^{ele}\} = \{F^e_\psi\} - \{F^e_{p.m}\} \end{aligned} \quad (9)$$

where, $[K^e_{uu}]$, $[K^e_{u\phi}]$, $[K^e_{u\psi}]$, $[K^e_{\phi\phi}]$, $[K^e_{\psi\psi}]$ and $[K^e_{\phi\psi}]$ are the elemental elastic stiffness matrix, elemental electro-elastic coupling stiffness matrix, elemental magneto-elastic coupling stiffness matrix, elemental electric stiffness matrix, elemental magnetic stiffness matrix and elemental electro-magnetic stiffness matrix, respectively. By employing the condensation procedure, Eq. (9) reduces to Eq. (10), which is solved to obtain nodal displacements. The detailed FE formulation and condensation procedure is similar to Vinyas and Kattimani [34].

$$[K_{eq}]\{u\} = \{F_{eq}\} \quad (10)$$

3. Results and Discussions

In the numerical calculation, a multiphase MEE beam with various volume fractions (V_f) of $BaTiO_3$ and $CoFe_2O_4$ is considered. The material properties corresponding to different V_f of $BaTiO_3$ and $CoFe_2O_4$ are listed in Kondaiah *et al.* [32]. The length of the multiphase MEE beam L = 1 m, width w = 0.1 m and thickness h = 0.1m. The influence of V_f and its corresponding coupled material properties on the direct and derived quantities of MEE beam are investigated across the beam thickness (at $x = L/2$). The thermo-mechanical load comprises of a uniform temperature load (10 K) and sinusoidally varying traction load. The influence of pyroeffects is also taken into account. Further, the numerical evaluation is carried out to investigate the effect of different mechanical load profiles on the displacements and potentials of thermal loaded MEE beam. In addition, effect of stacking sequence with respect to three layered BFB and FBF MEE beam is computed.

3.1. Validation of the formulation

The numerical example considered by Kondaiah *et al.* [32] is solved using the present finite element (FE) formulation. In order to validate with Kondaiah *et al.* [32], the effect of mechanical load is nullified in the formulation. The numerical evaluation using the present FE formulation is made for a multiphase MEE beam with V_f = 0.5. For the identical beam geometry and loading conditions, the results are compared with that of reported by Kondaiah *et al.* [32]. Figures 2(a) – (c) depict the validation of displacement component, electric potential and normal stress σ_x. It can be observed from these figures that there exists a good correlation between the two. Hence, it is justified that the present FE formulation is accurate.

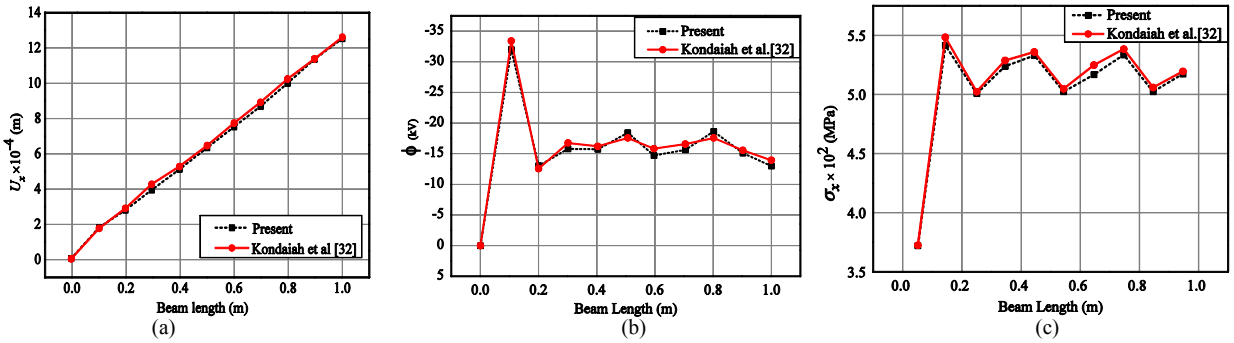

Fig. 2: Validation of (a) longitudinal x-direction (U_x) (b) electric potential (ϕ) (c) normal stress - σ_x

3.2. Effect of volume fraction

The volume fraction effect on a multiphase MEE cantilever beam is evaluated by considering a uniform temperature load of 10 K and sinusoidally varying traction load $q = q_0 \sin\left\{\frac{\pi x}{L}\right\}$ with amplitude $q_0 = 1500N$. Figs. 3(a) – (c) illustrate the effect of volume fraction on the longitudinal x-direction displacement component U_x, longitudinal y-direction displacement component U_v and transverse z-direction displacement component U_w, respectively. It may be observed from the Fig. 3(a) that a higher magnitude of U_x is attained for pure piezoelectric phase (V_f = 1.0). It is because of the lower values of elastic stiffness coefficients associated with V_f =1.0. From Figs. 3(b) and (c) it can be witnessed that the displacement components U_v and U_w follows a similar trend of variation with respect to volume fractions. The maximum U_v is witnessed at the bottom layer of MEE beam. Figure 4(a) illustrates the distribution of electric potential ϕ across the thickness of a multiphase MEE beam. It is also observed from this figure that the electric potential ϕ is higher for V_f = 0.2. This is due to the influence of pyroelectric effect. In addition, for all the volume fractions considered, the maximum value is observed at the top layer. Similarly, the magnetic potential distribution is depicted in Fig. 4(b). It can be seen that for V_f = 0.0 i.e. pure piezomagnetic phase, larger variation of magnetic potential ψ is observed. This may be due to higher values of piezomagnetic constants. For all the volume fractions, the normal stress σ_x varies linearly throughout the beam thickness as illustrated in Fig. 5(a). The maximum value of σ_x is witnessed at the top surface of the beam. It may be due to additional traction force

acting on the top surface of MEE beam, along with a uniform temperature load. Further, pure piezomagnetic phase has a higher stress value compared to remaining volume fractions. A similar trend of variation is observed for σ_y and σ_z. Hence, for the sake of brevity only the variation of σ_x is presented. The shear stress component τ_{xz} varies symmetrically across the beam thickness as shown in Fig. 5(b). It can also be seen that for all the volume fractions, the mid layer of MEE beam experiences maximum τ_{xz}. The variation of the electric displacement component in z-direction is illustrated in Fig. 6(a). It can be observed that D_z is zero for pure piezomagnetic phase and it is maximum for pure piezoelectric phase. It is because the value of piezoelectric co-efficient are zero for $V_f = 0.0$ and maximum for $V_f = 1.0$. As the piezoelectric constants of the corresponding V_f increases, the value of D_z increases. Similarly, for $V_f = 1.0$, the magnetic flux density is zero throughout the beam thickness and gradually increases with V_f approaching the pure piezomagnetic phase ($V_f = 0.0$) as illustrated in Fig. 6(b).

3.3. Layered MEE beams

In this section, the numerical evaluation is extended for layered MEE beam with three layers. The effect of stacking sequence on the direct quantities is analysed. The most commonly used stacking sequences such as *BFB* and *FBF* in which, *B* represents pure piezoelectric phase and *F* represents pure piezomagnetic phase are considered for the analysis. Also, the effect of different mechanical load profiles is evaluated for both layered and multiphase MEE beam. It is to be noted that the temperature load of 10 K is maintained while computing the effect of different mechanical loads. The various mechanical load profiles considered are as follows:

Sinusoidal load:

The mechanical load distribution is assumed to vary sinusoidally along the beam length. The general equation can be written as follows:

$$q = q_0 \sin\left\{\frac{\pi x}{L}\right\} \tag{11}$$

where, x is the distance from the clamped end and L is the beam length.

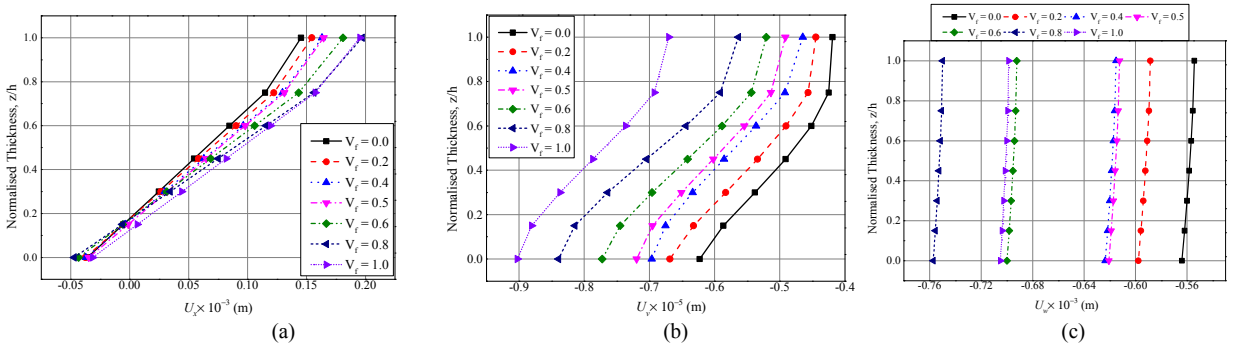

Fig. 3: Effect of volume fraction on (a) longitudinal displacement component U_x (b) longitudinal displacement component U_v (c) transverse displacement component U_w

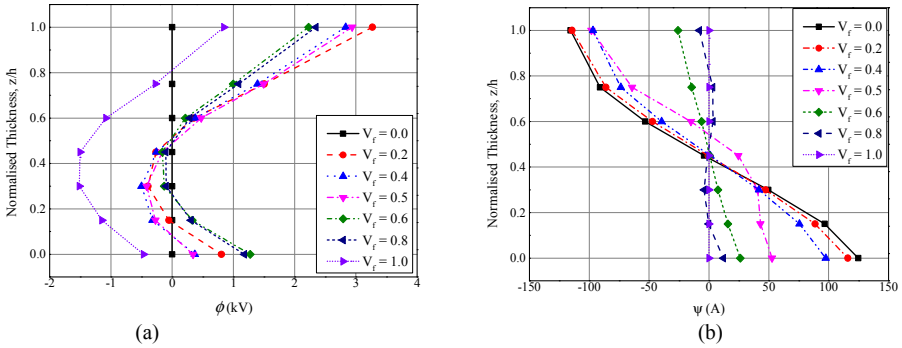

Fig. 4: Effect of volume fraction on (a) electric potential ϕ (b) magnetic potential ψ

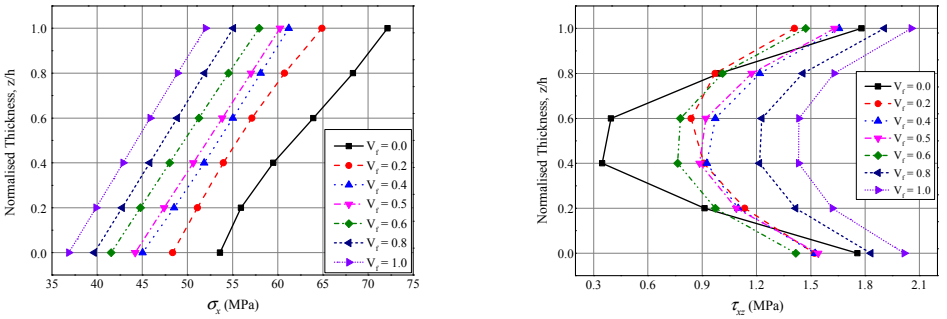

(a) (b)

Fig. 5: Effect of volume fraction on (a) normal stress σ_x (b) shear stress τ_{xz}

Uniformly distributed load (UDL):

The load intensity is assumed to be constant over the beam span with general equation

$$q = q_0 \tag{12}$$

In the present analysis, the magnitude of the load intensity is considered as $q_0 = 1500\ N$.

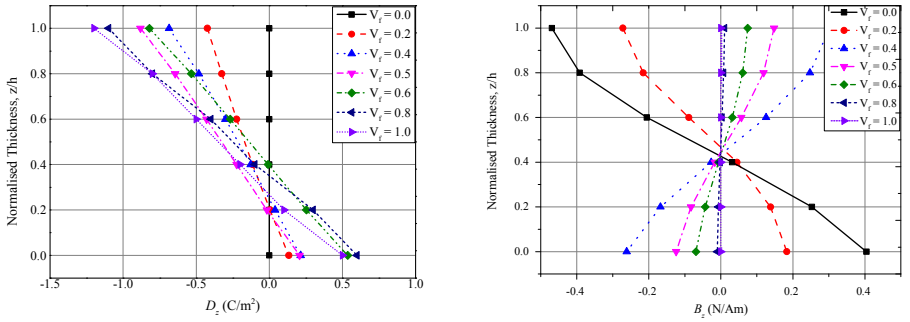

(a) (b)

Fig. 6: Effect of volume fraction on (a) electric displacement component D_z (b) magnetic flux density B_z

Uniformly varying load (UVL):

In this case, the load along the beam length varies according to the general equation

$$q = q_0 \left\{\frac{x}{L}\right\} \tag{13}$$

Figure (7) compares the effect of stacking sequence on the transverse z-direction displacement component U_w. It is noticed from this figure that for both the stacking sequence, UDL has a significant effect on U_w across the beam thickness. Further, BFB stacking sequence results in a higher displacement than FBF stacking sequence. This may be due to the presence of two layers of pure piezoelectric (B) material which reduces the stiffness of MEE beam. The magnetic potential ψ variation along the thickness direction for BFB and FBF MEE beam is shown in Figs. 8(a) and (b), respectively. It is observed that the variation is quite different for both the stacking sequences. For BFB-MEE beam, the ψ is almost invariant at the top and bottom layer since it is made of pure piezoelectric phase. Similarly for FBF stacking sequence the ψ varies linearly at each layer due to the coupling between piezoelectric and piezomagnetic phases at the interface. Also, the variation of the electric potential ϕ is displayed in Figs. 9(a) and (b) for BFB and FBF stacking sequence, respectively. The above mentioned explanation for ψ holds good for ϕ also. Further, for both the potentials negligible effect of mechanical loading profiles is witnessed.

For a multiphase MEE beam the effect of thermo-mechanical load profiles *viz.* sinusoidal, UDL and UVL on the maximum values of the direct quantities are investigated. Tables (1) and (2) encapsulate the maximum U_x, U_v, U_w , ϕ and ψ for a multiphase MEE beam with different volume fraction. It can be observed that UDL profile has a significant effect on the multilayered MEE beam.

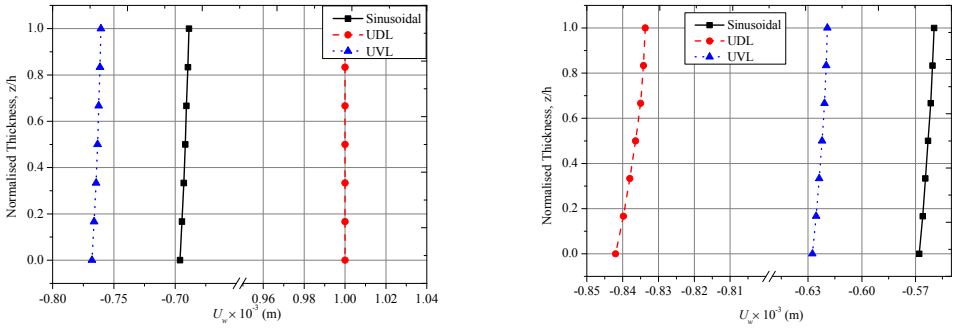

Fig. 7: Effect of mechanical loading profiles on transverse *z*-direction displacement component (a) BFB (b) FBF MEE beam

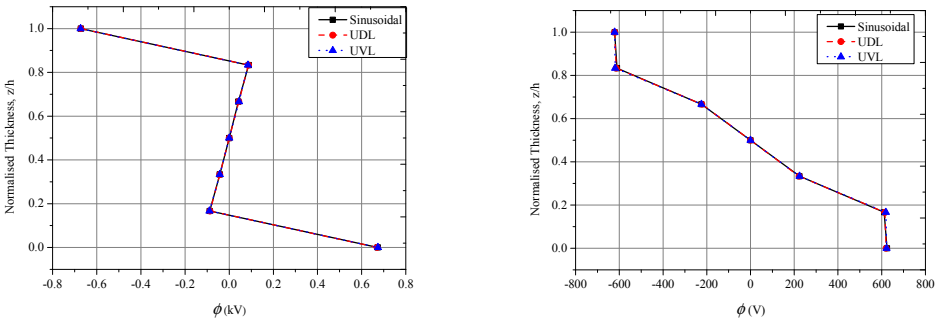

Fig. 8: Effect of mechanical loading profiles on magnetic potential ψ (a) BFB (b) FBF MEE beam

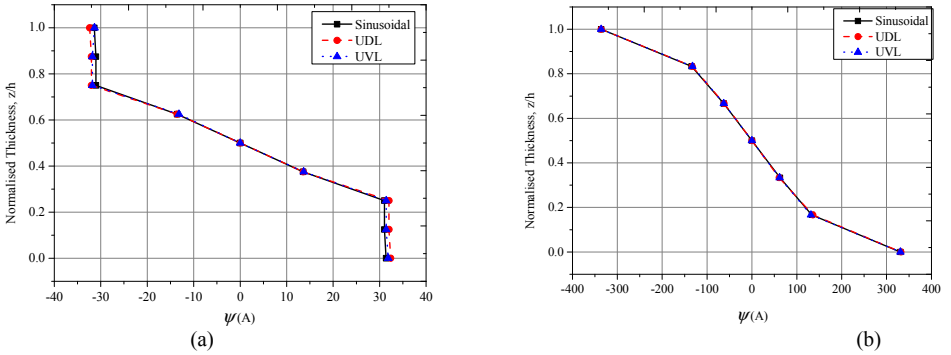

Fig. 9: Effect of mechanical loading profiles on electric potential ϕ (a) BFB (b) FBF MEE beam

Table 1: Effect of mechanical loading profiles on longitudinal *x*-direction displacement U_x, *y*-direction displacement U_v and transverse *z*-direction displacement U_w

	Max. U_x (10^{-3} m)			Max. U_v (10^{-5} m)			Max. U_w (10^{-3} m)		
Volume fraction (V_f)	*Sinusoidal*	*UDL*	*UVL*	*Sinusoidal*	*UDL*	*UVL*	*Sinusoidal*	*UDL*	*UVL*
0	0.145	0.19	0.16	-0.62	-0.70	-0.68	-0.56	-0.84	-0.62
0.2	0.154	0.20	0.17	-0.67	-0.76	-0.73	-0.60	-0.86	-0.66
0.4	0.163	0.21	0.18	-0.70	-0.79	-0.76	-0.62	-0.92	-0.69
0.6	0.18	0.24	0.20	-0.77	-0.87	-0.84	-0.70	-1.04	-0.77
0.8	0.19	0.26	0.22	-0.84	-0.95	-0.91	-0.75	-1.12	-0.84
1.0	0.2	0.28	0.23	-0.90	-1.00	-0.96	-0.77	-1.17	-0.89

Table 2: Effect of mechanical loading profiles on the maximum electric potential ϕ and magnetic potential ψ

	Max. ϕ (kV)			Max. ψ (A)		
Volume fraction (V_f)	*Sinusoidal*	*UDL*	*UVL*	*Sinusoidal*	*UDL*	*UVL*
0	0	0	0	124.0	127.08	126.0
0.2	3.27	4.42	4.01	115.9	117.4	116.3
0.4	2.83	3.84	3.52	-98.18	-106.96	-99.22
0.6	2.22	3.28	2.92	26.10	28.40	27.12
0.8	2.34	3.77	3.42	11.75	13.81	12.32
1.0	-1.5	3.18	2.82	0	0	0

Conclusions

In this paper, the static behavior study of a multiphase MEE beam with different volume fraction (V_f) is carried out. In this regard, a finite element formulation is developed and implemented with the help of a MATLAB code. The numerical evaluation reveals that the displacement components are higher for the pure piezoelectric phase (V_f = 1.0) whereas, a dominant effect of pure piezomagnetic phase (V_f = 0.0) is observed on the stress across the beam thickness. Due to the influence of the pyroeffects, the maximum electric potential is witnessed for V_f = 0.2. The maximum magnetic potential is observed for V_f = 0.0, as it has a higher piezomagnetic coefficients. Further, for a multiphase magneto-electro-elastic beam, the maximum electric displacement component D_z and the maximum magnetic flux density component B_z is noticed for pure piezoelectric and pure piezomagnetic phase, respectively. For the layered MEE beam, BFB stacking sequence has more impact on the displacement components. As a result of higher number of pure piezoelectric and pure piezomagnetic layers in the corresponding stacking sequence, BFB and FBF stacking sequence results in a higher electric and magnetic potential, respectively. Among all the forms of mechanical loads considered, UDL has a prominent on the displacement components whereas, an insignificant effect on the potentials of the system is noticed.

References

[1]. Hadjiloizi DA, Georgiades AV, Kalamkarov AL, Jothi S, European Journal of Mechanics A/Solids 2013; 39: 298-312.
[2]. Tian Tang, Wenbin Yu, Smart Materials and Structures 2009; 18: 125026.
[3]. Miara B , Rohan E , Griso G , Avila A , Bossavit A , Ouchetto O , Zouhdi S , Zidi M, Labat B, Mechanics of Advanced Materials and Structures 2007; 14(1): 33-42.
[4]. Pan E, Heyliger H, Journal of Sound and vibration 2002; 252(3): 429-442.
[5]. Fernando Ramirez, Paul R Heyliger, Ernian Pan, Journal of Sound and Vibration 2006; 292: 626–644.
[6]. Milazzo A, Orlando C, Alaimo A, Smart Materials and Structures 2009; 18(8): 85012.
[7]. Jiang A, Ding H, Structural Engineering and Mechanics 2004; 18: 195–209.
[8]. Annigeri AR, Ganesan N, Swarnamani S, Journal of Sound and Vibration 2007; 299: 44–63.
[9]. Rajesh K Bhangale, Ganesan N, Journal of Sound and Vibration 2006; 294: 1016-1038.
[10]. Libo Xin, Zhendong Hu, Composite Structures 2015; 125: 96-103.
[11]. Chen WQ, Lee KY, Ding HJ, Journal of Sound and Vibration 2005; 279: 237-251.
[12]. Chen J, Chen H, Pan E. Heyliger PR, Journal of Sound and Vibration 2007; 304(3-5): 722–734.
[13]. Kattimani SC, Ray MC, Composite Structures 2014; 14: 51-63.
[14]. Kattimani SC, Ray MC, International Journal of Mechanics and Materials in Design 2014; 10(4): 351–378.
[15]. Kattimani SC, Ray MC, International Journal of Mechanical Sciences 2015; 99: 154–167.
[16]. Wu CP, Lu CY, Composite Structures. 2009; 90: 363–372.
[17]. Biju B, Ganesan N, Shankar K, IEEE Sensors Journal 2011; 11(9): 2169–2176.
[18]. Hou PF, Leung AYT, Smart Materials and Structures 2004, 13: 762–776.
[19]. Hou PF, Ding HJ, Leung AYT, Journal of Sound and Vibration 2006; 291: 19–47.
[20]. Daga A, Ganesan N, Shankar K, Journal of Mechanics of Materials and Structures 2008; 3(2): 375–390.
[21]. Daga A, Ganesan N, Shankar K, International Journal for Computational Methods in Engineering Science and Mechanics 2009; 10(3): 173-185.
[22]. Phoenix SS, Satsangi SK, Singh BN, Journal of Sound and Vibration 2009; 324 (3-5): 798–815.
[23]. Giuseppe Davi, Alberto Milazzo, Calogero Orlando, Mechanics of Advanced Materials and Structures 2008; 15(3-4): 220-227.
[24]. Garcia Lage R, Mota Soares CM, Mota Soares CA, Reddy JN, Computers & Structures 2004; 82: 1293–1301.
[25]. Sunar M, Ahmed Z Al-Garni, Ali MH, Kahraman R, AIAA Journal 2002; 40: 1845-1851.
[26]. Thar M Badri, Hussain H Al-Kayiem. Asian journal of scientific research 2013; 6: 236-244.
[27]. Tauchert TR, Journal of Thermal Stresses 1996; 19: 287-296.

[28]. Farzad Ebrahimi, Mohammad Reza Barati, Applied Physics-A 2016; 122: 451.
[29]. Farzad Ebrahimi, Mohammad Reza Barati, International Journal of Smart and Nano Materials 2016; 7(2): 69-90.
[30]. Kumaravel A, Ganesan N, Sethuraman R, Smart Materials and Structures 2007; 16(2): 282–295.
[31]. Kondaiah P, Shankar K, Ganesan N, Smart Materials and Structures 2013; 22: 025007.
[32]. Kondaiah P, Shankar K, Ganesan N, Coupled Systems Mechanics 2012; 1(2): 205-217.
[33]. Kondaiah P, Shankar K, Ganesan N, Coupled Systems Mechanics 2013; 2: 1-22.
[34]. Vinyas M, S.C. Kattimani, Composite structures2017; 163: 216-237.